Journal of Solar Energy Research (JSER)

Optimization of Structure of Solar Cells Based on Lead Perovskites (CH₃NH₃PbX₃, X: I, Br) Via Numerical Simulation

Farzad Sadeghi[a,*], Mina Neghabi[b]

[a] Center for Advanced Engineering Research, Majlesi Branch, Islamic Azad University, Majlesi, Iran
[b] Department of Physics, Faculty of Science, Najafabad Branch, Islamic Azad University, Najafabad, Iran

ARTICLE INFO

Keywords:

ABSTRACT

In this paper, numerical simulation of perovskite solar cells (PSCs) for two structures (direct and inverted) and two perovskites (MAPbX$_3$, MA: CH$_3$NH$_3$, X: I, Br) had been done by SCAPS software. Thickness of active layers (the perovskites) have been optimized by using PCE curves and then, electrical properties of the solar cells have been extracted. Results of simulations show that the best structure is inverted structure with active layer MAPbI$_3$ which characteristics of the structure are 15.4%, 24.68 mA/cm^2, 8.48 V, and 73.74% for PCE, J$_{SC}$, V$_{OC}$, and FF, respectively. In addition, study of donors or acceptors density demonstrate that the parameter is so effective on performance of solar cells and PCE achieved to 18% by increase in the parameter.

1. Introduction

In the recent years, organic – inorganic perovskite hybrids with structure ABX$_3$ (A: CH3NH$_3$, B: Pb, Sn and X: I, Br) are considered by scientists [1-4]. Achievement to 21% of power conversion efficiency (PCE) in 2016 during seven years of development of them in comparison with 3.8% of PCE in the first report in 2009 shown a new and promising generation of solar cells based on the perovskites which have cheaper and easier process of fabrication than past generations of solar cells [3, 5-10]. Additionaly, other parameters of perovskites for instance high absorption coefficient, good ability in carrier transmission, fabrication in low temperatures and low sensitivity in defects of crystals prepared possibility of fabrication of solar cells with PCE around 20% by the absorbers [2, 6, 8, 11].

Recently, several simulations for pervoskite solar cells (PSCs) hace been carried out and in most of them, only a perovskite or only a structure (direct or invested) has been studied. In 2014, Chang and et al [1] did an optical simulation for tandem solar cells with CH$_3$NH$_3$PbI$_{3-x}$Cl$_x$ in active layer and they found 29% of PCE. A 2-dimnetional electrical and optical simulation for CH$_3$NH$_3$PbI$_3$ solar cell has been done by Kian Jo et al [12] in 2015. Hossein et al [7], in 2015, carried out a numerical simulation for CH$_3$NH$_3$PbI$_3$

perovskite solar cell and results shown a 24% of PCE. Also, in 2015, Yadef and et al [13] did two simulations by two various software packages; The results have good agreement with experimental data. Again, Sun and et al [14], in 2015, presented an analytical solution for p-p-n, n-p-p, p-i-n, and n-i-p perovskite solar cells. Finally, in 2016, Jang and et al [11] figured out a simulation for two CH₃NH₃PbI₃ and CH₃NH₃PbBr₃ perovskites by numerical methods which report a 27.5% of PCE for CH₃NH₃PbI₃.

In this study, electrical simulations of PSCs for two perovskites (MAPbX3, X: I, Br) and two structures (direct and inverted) are studied. General comparison between structures and perovskites is presented. Numerical simulations have been done by SCAPS software which developed in Computer and Informatics faculty of university of Gent in Belgium [15]. Thickness of perovskite layers of PSCs have been optimized by PCE curves and then, parameters of J$_{SC}$, V$_{OC}$, and FF of the cells have been extracted. Finally, achieved results for various structures have been compared and the best structure has been determined, and also parameter of donors or acceptors density has been studied.

2. Theory

One dimensional equations which describe holes and electrons behavior in semiconductors is a Poison equation as follow:

$$\frac{\partial^2}{\partial x^2}\psi(x) = \frac{q}{\epsilon}(N(x) + n(x) - p(x)) \qquad (1)$$

where q unit of electrical charge, ε dielectric constant, ψ ectrical potential, doping density, and n and p are electron and hole densities. Equations of current densities of electrons and holes are:

$$J_n = J_{diffusion} + J_{drift} = qD_n\frac{\partial n}{\partial x} + \mu_n qn\frac{\partial \psi}{\partial x}, \qquad (2)$$

$$J_p = -qD_p\frac{\partial p}{\partial x} + \mu_p qp\frac{\partial \psi}{\partial x} \qquad (3)$$

where $\mu_{n(p)}$ mobility, $D_{n(p)}$ diffusion coefficient and n and p are symbols for electrons and holes. Parameters of $\mu_{n(p)}$ and $D_{n(p)}$ satisfy Einstein's relation:

$$\frac{D_n}{\mu_n} = \frac{D_p}{\mu_p} = \frac{k_B T}{q} \qquad (4)$$

where k_B and T are Boltzmann's constant and temperature, respectively. Additionally, in steady conditions, continuous equations of current density are:

$$-\frac{1}{q}\frac{dJ_n}{dx} = G - R, \qquad (5)$$

$$\frac{1}{q}\frac{dJ_p}{dx} = G - R, \qquad (6)$$

where G is rate of carrier generation and R is recombination rate of electrons and holes.

3. Simulation method and required parameters

In this paper, numerical simulation of PSCs for direct (p-p-n) and inverted (n-p-p) structures and two perovskites (MAPbX3, X: I, Br) has been done by SCAPS. Thus, four structures are categorized to A, B, C, and D as follow which are presented in table 1. For optimization of thickness of perovskite layers, owing to importance of PCE factor in comparison of solar cells, PCE curves have been plotted versus thickness of perovskite layer from 50 to 1000 nm. Then, optimum thickness of perovskite layers are chosen where PCEs are maximum. In addition, cost issues and technical problems are considered.

Table 1. Category of structures		
Type	**Symbol**	**Structure**
Direct	A	ITO(120 nm) / PEDOT:PSS (50 nm) / MAPbI3 (x) / PCBM (50 nm) /Al(100 nm)
Direct	B	ITO(120 nm) / PEDOT:PSS (50 nm) / MAPbBr3 (x) / PCBM (50 nm) /Al(100 nm)
Inverted	C	ITO(120 nm) / TiO2 (50 nm) / MAPbI3 (x) / Spiro-OMeTAD (200 nm) /Al(100 nm)
Inverted	D	ITO(120 nm) / TiO2 (50 nm) / MAPbBr3 (x) / Spiro-OMeTAD

		(200 nm) /Al(100 nm)

Molecular properties of materials are needed for electrical simulation. Some parameters extract from previous studies (the refrences have been presented in tables) and some of them have been calculated theoretically. Molecular properties of materials in p-n junctions are in table 2 and some structural parameters in active layers are in table 3.

Table 2. Required parameters for PCBM, TiO2, MAPbI3, and MAPbBr3

Parameters	MAPbI3	MAPbBr3
Electron thermal velocity (cm/s)	2.4E18	2.4E18
Hole thermal velocity (cm/s)	2.4E18	1.6E18
Electron capture cross (cm^2)	1E-16	1E-16
Hole capture cross (cm^2)	1E-16	1E-16
Exciton lifetime (ns)	16 [24]	22 [24]
Total defect (cm^{-3})	2.6E18	2.2E18
Radiative recombination coefficient (cm^3/s)	1.5E-10 [25]	4.9E-10 [25]
Auger electron capture coefficient (cm^6/s)	3.4E-28 [25]	13.5E-28 [25]
Auger hole capture coefficient (cm^6/s)	3.4E-28 [25]	13.5E-28 [25]
Electron effective mass	0.23 [5]	0.50 [5]
Hole effective mass	0.29 [5]	0.23 [5]

For confirmation and validation of simulation results, a simulation has been carried out for a direct structure which has been fabricated by Sun and et al [16].

Geometry of the structure is as ITO (150 nm) /

PEDOT:PSS (50 nm) / MAPbI3 (50 nm) / PCBM (50 nm) / Al (150 nm). Figure 1 shows comparison between current density - voltage curve (J-V) of experimental data and simulation of the direct structure by SCAPS which displays a good agreement. In addition,

table 4 shows solar cell characteristics for simulation and experimental data.

Table 3. Required structural parameters of perovskites

Parameters	Symbol	PCBM	TiO₂	MAPbBr₃	MAPbI₃
Band gap (eV)	E_g	2.1 [17]	3.2 [12]	2.33 [18]	1.50 [12]
Affinity (eV)	χ	3.90 [17]	4.0 [12]	3.70 [19]	3.93 [12]
Relative dielectric	ε_r	3.90 [20]	9 [12]	7.50 [21]	6.50 [12]
Effective density of states in conduction band (1/cm^3)	N_C	1E21 [17]	1E19 [12]	1E17 [21]	2.2E18 [12]
Effective density of states in valence band (1/cm^3)	N_V	1E21 [17]	1E19 [12]	1E17 [21]	1.8E19 [12]
Electron mobility (cm^2/Vs)	μ_e	1 [16]	2E-2 [12]	24 [22]	0.50 [12]
Hole mobility (cm^2/Vs)	μ_h	0.21 [23]	2 [12]	24 [22]	0.50 [12]
Acceptor density (1/cm^3)	N_A	1E21 [17]	----	1E16 [21, 22]	1E13 [12]
Donor density (1/cm^3)	N_D	----	1E19 [12]	1E16 [21, 22]	1E13 [12]

Table 4. Comparison between experimental and simulation for a direct structure

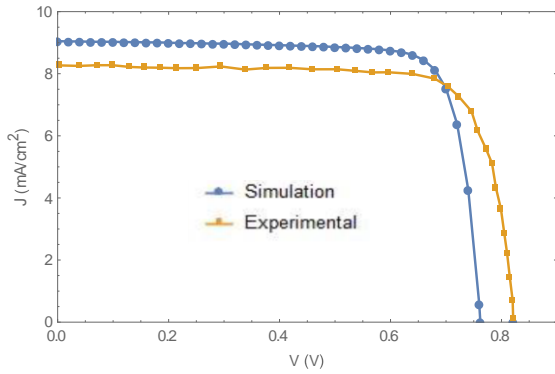| Parameters	PCE	Jsc	Voc	FF
Experimental	5.2	8.2	0.82	77.00
Simulation	5.5	9.00	0.78	80.80

317

Figure 1. J-V curves of experimental data [16] and simulation for a direct structure

4. Simulation results

4.1. PSCs optimization

Figure 2 has shown curves of PCE versus thickness of perovskite for different structures. The curves illustrate that all structures are optimized in around many hundreds of nanometers of thickness which were predictable according to high diffusion length of perovskite materials. In all structures, thickness of layers of PCBM, TiO$_2$, PEDOT:PSS, and Spiro-OMeTAD have been examined and the results shown that their thicknesses do not have imppressive effect on PCE of PSCs. Thus, considering economical aspects, 50 nm of thickness was selected for PCBM, TiO$_2$, and PEDOT:PSS and 200 nm for Spiro-OMeTAD in simulations.

Variations of PCE curves show that MAPbI$_3$ has higher PCE than MAPbBr$_3$. Lower energy band gap and higher absorption of MAPbI$_3$ are effective on the result. Therefore, structures A and C have higher PCEs. In addition, because of structure type, various diffusion length, different recombination coefficients, and defects, PCE of any structure is optimized in a special thickness. If thickness is more or less than optimum amount, PCE will decline owing to increase in defects and recombination or decrease in generation rate of carriers and lower optical absorption, respectively.

Results show that structures A, B, and C are optimized around 250, 400, 275 nm which have 13%, 11%, and 15.4% of PCE, respectively. Also, structure D has a peak on 1500 nm but PCE of the structure varies in order of hundredth from 800 to 1500 nm. Thus, optimum thickness is considered 800 nm

which has 11.5% of PCE. PCE curves illustrate that structures C and D are the best and the worst, respectively, which both belong to inverted structure and this result shows that type of perovskite is so more important for PSCs than type of structure. Additionally, due to lower band gap and higher absorption coefficient, MAPbI$_3$ has better performance than MAPbBr$_3$.
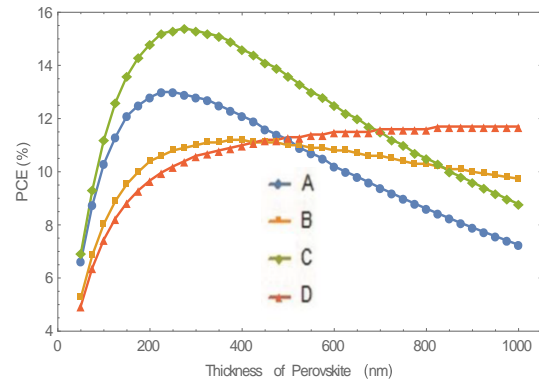

Figure 2. Changes of PCE vs thickness of perovskites for A, B, C, and D structures

4.2. J-V curves and characteristics of the cells

Geometry of structures are completed by optimum thicknesses which are found in simulations. Thus, J-V curves of structures can be ploted and the parameters of the cells are extracted. Figure 3 show J-V curves for the structures A, B, C, and D. Characteristics of the solar have been presented in table 5.

4.3. Examination of total defects, radiative recombination coefficient, and donor and acceptor densities

In this section, three vital factors which affect PCE of solar cells are studied.

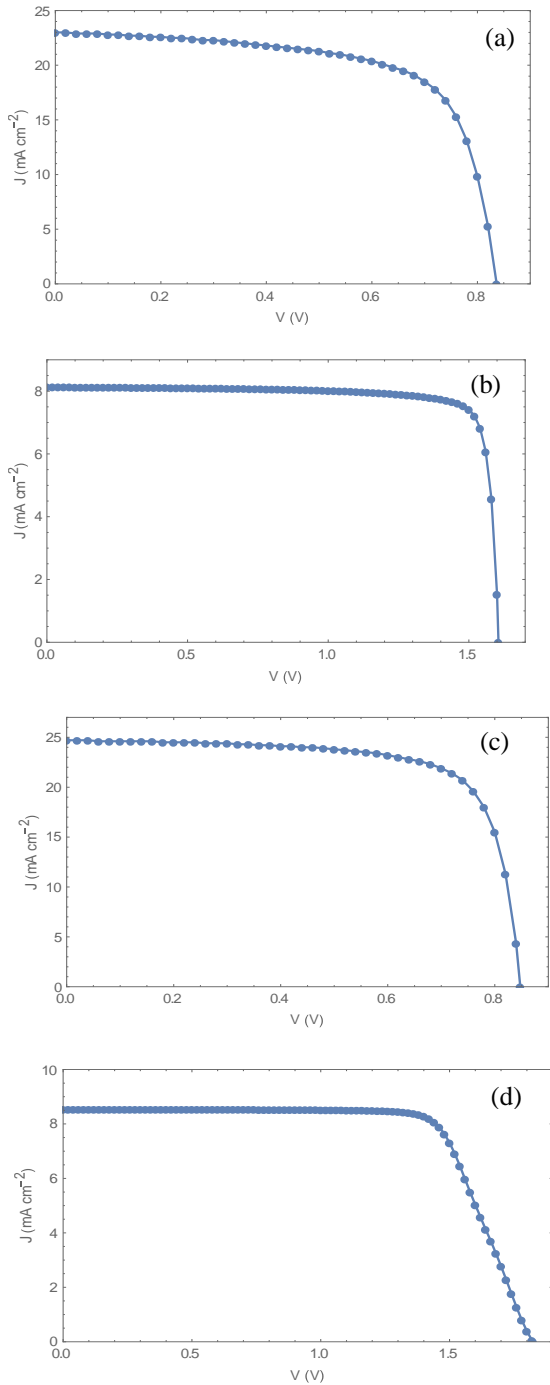| Table 5. Achieved parameters of simulation of structures				
Structure	**Direct**		**Inverted**	
Symbol	**A**	**B**	**C**	**D**
VOC (V)	0.83	1.61	8.48	1.82
JSC (mA/cm2)	23.00	8.14	24.68	8.54
FF (%)	67.50	88.35	73.74	74.74
PCE (%)	13.00	11.15	15.40	11.65

Figure 3. J-V curves of, a) structure A, b) structure B, c) structure C, and d) structure D

According to found results in two previous sections, these factors are examined for two structures A and C which had higher PCE. Fig.4 illustrate variation of PCE versus variation of total defect (N_t) from 10^{17} to 10^{19} ($1/cm^{-3}$) to show an increase 0.5% for structure A and 1.5% for structures C. Figure 5 show that PCEs are almost fix for variations of radiative recombination coefficient from 10^{-}

^{12} to 10^{-8} (cm^3/s). Changes of donor or acceptor densities is so vital parameter to influence on PCE of solar cells. Variation of the parameter from 10^{12} to 10^{15} ($1/cm^{-3}$) illustrates that PCEs reach 14% and 18% for structures A and C, respectively, which has present in Figure 6.
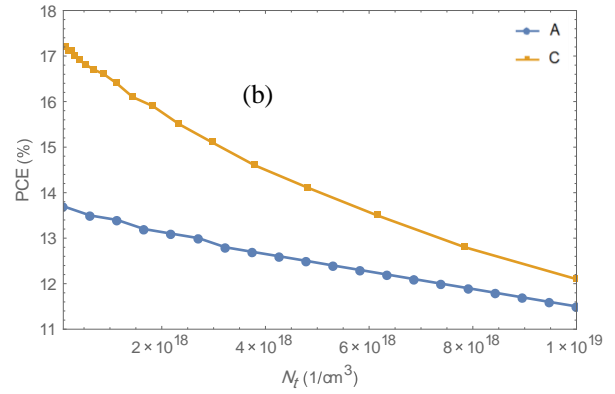

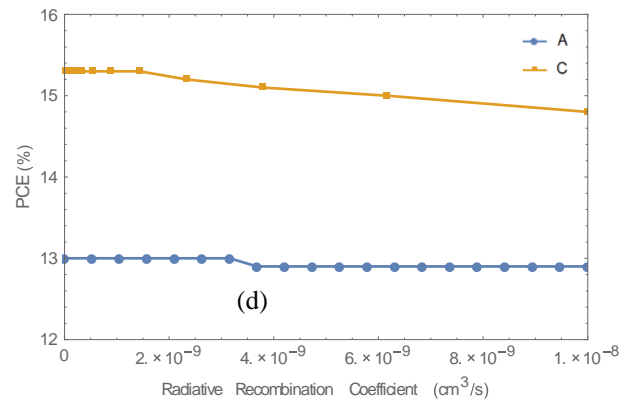Figure 4. Variations of PCE vs changes of total defect from 10^{17} to 10^{19}

Figure 5. Variations of PCE vs changes of radiative recombination coeficient from 10^{-12} to 10^{-8}
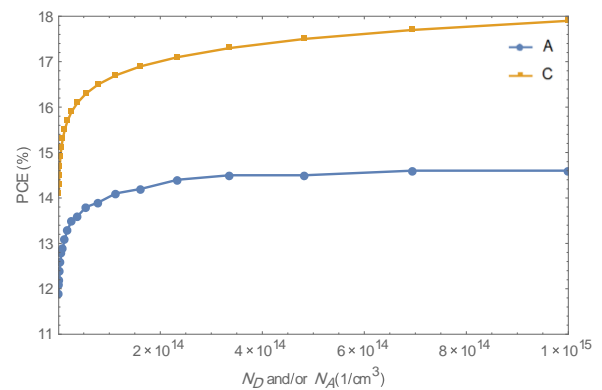

Figure 6. Variations of PCE vs changes of density of donors and / or acceptors from 10^{12} to 10^{15}

5. Conclusion

Numerical simulation of perovskite solar cells (PSCs) for two structures (direct and inverted) and two perovskites (MAPbX$_3$, MA: CH3NH$_3$, X: I, Br) have been done by PCE curves. Achieved results show that optimized thickness for structures A (ITO(120 nm) / PEDOT:PSS (50 nm) / MAPbI$_3$ (x) / PCBM (50 nm) /Al(100 nm)), B (ITO(120 nm) / PEDOT:PSS (50 nm) / MAPbBr$_3$ (x) / PCBM (50 nm) /Al(100 nm)), C (ITO(120 nm) / TiO$_2$ (50 nm) / MAPbI$_3$ (x) / Spiro-OMeTAD (200 nm) /Al(100 nm)), and D (ITO(120 nm) / TiO$_2$ (50 nm) / MAPbBr$_3$ (x) / Spiro-OMeTAD (200 nm) /Al(100 nm)) are 250, 400, 275, and 800 nm, respectively. Comparison between operations of structures illustrate that inverted structure has better performance. Also, MAPbI$_3$ shows better behavior for PSCs due to higher absorption and lower band gap. Structure C illustrates the best performance and achieve to 15.5% of PCE. In addition, variation of total defects, radiative recombination coefficient, and donor and acceptor densities shows that the PCE can increase to 18% for structure C.

Acknowledgment

References

[1]C.-W. Chen, S.-Y. Hsiao, C.-Y. Chen, H.-W. Kang, Z.-Y. Huang and H.-W. Lin. (2015). Optical properties of organometal halide perovskite thin films and general device structure design rules for perovskite single and tandem solar cells, 3, 9152-9159.
[2]M. J. Taghavi, M. Houshmand, M. H. Zandi and N. E. Gorji. (2016). Modeling of optical losses in perovskite solar cells, 97, 424-428.
[3]Z.-L. Huang, C.-M. Chen, Z.-K. Lin and S.-H. Yang. (2017). Efficiency enhancement of regular-type perovskite solar cells based on Al-doped ZnO nanorods as electron transporting layers, 102, 94-102.
[4]R. Pandey and R. Chaujar. (2016). Numerical simulations: Toward the design of 27.6% efficient four-terminal semi-transparent perovskite/SiC passivated rear contact silicon tandem solar cell, 100, 656-666.
[5]G. Berdiyorov, F. El-Mellouhi, M. Madjet, F. Alharbi, F. Peeters and S. Kais. (2016). Effect of halide-mixing on the electronic transport properties of organometallic perovskites, 148, 2-10.
[6]H. Hoppe, N. Sariciftci and D. Meissner. (2002). Optical constants of conjugated polymer/fullerene based bulk-heterojunction organic solar cells, 385, 113-119.
[7]M. I. Hossain, F. H. Alharbi and N. Tabet. (2015). Copper oxide as inorganic hole transport material for lead halide perovskite based solar cells, 120, 370-380.
[8]Z. Xiao, Y. Yuan, Q. Wang, Y. Shao, Y. Bai, Y. Deng, Q. Dong, M. Hu, C. Bi and J. Huang. (2016). Thin-film semiconductor perspective of organometal trihalide perovskite materials for high-efficiency solar cells, 101, 1-38.
[9]A. Baktash, O. Amiri and A. Sasani. (2016). Improve efficiency of perovskite solar cells by using magnesium doped ZnO and TiO 2 compact layers, 93, 128-137.
[10]H. Faltakh, M. Mahdouani, I. Hemdana, S. B. Dkhil, R. Bourguiga and J. Davenas. (2015). Extraction of different parameters of hybrid solar cell based on PVK/Silicon nanowires, 79, 166-179.
[11]A. Zhang, Y. Chen and J. Yan. (2016). Optimal Design and Simulation of High-Performance Organic-Metal Halide Perovskite Solar Cells, 52, 1-6.
[12]Q. Zhou, D. Jiao, K. Fu, X. Wu, Y. Chen, J. Lu and S.-e. Yang. (2016). Two-dimensional device modeling of CH 3 NH 3 PbI 3 based planar heterojunction perovskite solar cells, 123, 51-56.
[13]P. Yadav, K. Pandey, P. Bhatt, D. Raval, B. Tripathi, M. K. Pandey and M. Kumar. (2015). Exploring the performance limiting parameters of perovskite solar cell through experimental analysis and device simulation, 122, 773-782.
[14]X. Sun, R. Asadpour, W. Nie, A. D. Mohite and M. A. Alam. (2015). A Physics-Based Analytical Model for Perovskite Solar Cells, 5, 1389-1394.

[15]. http://scaps.elis.ugent.be

[16]S. Sun, T. Salim, N. Mathews, M. Duchamp, C. Boothroyd, G. Xing, T. C. Sum and Y. M. Lam. (2014). The origin of high efficiency in low-temperature solution-processable bilayer organometal halide hybrid solar cells, 7, 399-407.

[17]K. Akaike, K. Kanai, H. Yoshida, J. y. Tsutsumi, T. Nishi, N. Sato, Y. Ouchi and K. Seki. (2008). Ultraviolet photoelectron spectroscopy and inverse photoemission spectroscopy of [6, 6]-phenyl-C61-butyric acid methyl ester in gas and solid phases, 104, 023710.

[18]C. Wehrenfennig. (2014). Ultrafast spectroscopy of charge separation, transport and recombination processes in functional materials for thin-film photovoltaics: University of Oxford.

[19]J. Endres, D. A. Egger, M. Kulbak, R. A. Kerner, L. Zhao, S. H. Silver, G. Hodes, B. P. Rand, D. Cahen and L. Kronik. (2016). Valence and Conduction Band Densities of States of Metal Halide Perovskites: A Combined Experimental–Theoretical Study, 7, 2722-2729.

[20]V. D. Mihailetchi, J. K. van Duren, P. W. Blom, J. C. Hummelen, R. A. Janssen, J. M. Kroon, M. T. Rispens, W. J. H. Verhees and M. M. Wienk. (2003). Electron transport in a methanofullerene, 13, 43-46.

[21]N. Kedem, T. M. Brenner, M. Kulbak, N. Schaefer, S. Levcenko, I. Levine, D. Abou-Ras, G. Hodes and D. Cahen. (2015). Light-induced increase of electron diffusion length in ap–n junction type CH3NH3PbBr3 perovskite solar cell, 6, 2469-2476.

[22]M. I. Saidaminov, A. L. Abdelhady, B. Murali, E. Alarousu, V. M. Burlakov, W. Peng, I. Dursun, L. Wang, Y. He and G. Maculan. (2015). High-quality bulk hybrid perovskite single crystals within minutes by inverse temperature crystallization, 6.

[23]P. H. Wöbkenberg, D. D. Bradley, D. Kronholm, J. C. Hummelen, D. M. de Leeuw, M. Cölle and T. D. Anthopoulos. (2008). High mobility n-channel organic field-effect transistors based on soluble C 60 and C 70 fullerene derivatives, 158, 468-472.

[24]L. Kong, G. Liu, J. Gong, Q. Hu, R. D. Schaller, P. Dera, D. Zhang, Z. Liu, W. Yang and K. Zhu. (2016). Simultaneous band-gap narrowing and carrier-lifetime prolongation of organic–inorganic trihalide perovskites, 113, 8910-8915.

[25]Y. Yang, M. Yang, Z. Li, R. Crisp, K. Zhu and M. C. Beard. (2015). Comparison of recombination dynamics in CH3NH3PbBr3 and CH3NH3PbI3 perovskite films: Influence of exciton binding energy, 6, 4688-4692.